A new methodology for PBL height estimations based on lidar depolarisation measurements: analysis and comparison against MWR and WRF model based results

Juan Antonio Bravo-Aranda[1,2,a], Gregori de Arruda Moreira[3], Francisco Navas-Guzmán[4], María José Granados-Muñoz[1,2,b], Juan Luis Guerrero-Rascado[1,2], David Pozo-Vázquez[5], Clara Arbizu-Barrena[6], Francisco José Olmo Reyes[1,2], Marc Mallet[7,c] and Lucas Alados Arboledas[1,2]

[1]Andalusian Institute for Earth System Research (IISTA-CEAMA), Granada, Spain
[2]Dpt. Applied Physics, University of Granada, Granada, Spain
[3]Institute of Energetic and Nuclear Research (IPEN), São Paulo, Brazil
[4]Institute of Applied Physics (IAP), University of Bern, Bern, Switzerland
[5]Dpt. of Physics, University of Jaén, Jaén, Spain
[6]Laboratoire d'Aérologie, Toulouse, France
[7]Centre National de Recherches Météorologiques, Toulouse, France
[a]now at: Institute Pierre-Simon Laplace, CNRS-Ecole Polytechnique, Paris, France
[b]currently at: Table Mountain Facility, NASA/Jet Propulsion Laboratory, California Institute of Technology, Wrightwood, California, USA
[c]now at: CNRM, Météo-France-CNRS, Toulouse, France

Correspondence to: Juan A. Bravo-Aranda (jabravo@ugr.es)

Abstract.

The automatic and non-supervised detection of the planetary boundary layer height (z_{PBL}) by means of lidar measurements was widely investigated during the last years. Despite considerable advances, the experimental detection still presents difficulties such as advected aerosol layers coupled to the PBL which usually produce an overestimation of the z_{PBL}. To improve the detection of the z_{PBL} in these complex atmospheric situations, we present a new algorithm, called POLARIS (PBL height estimatiOn based on Lidar depolARISation). POLARIS applies the wavelet covariance transform (WCT) to the range corrected signal (RCS) and to the perpendicular-to-parallel signal ratio (δ) profiles. Different candidates for z_{PBL} are chosen and the selection is done, based on the WCT applied to the RCS and the δ. We use two ChArMEx campaigns with lidar and microwave radiometer (MWR) measurements, conducted on 2012 and 2013, for the POLARIS' adjustment and validation. POLARIS improves the z_{PBL} detection compared to previous methods based on lidar measurements, especially when an aerosol layer is coupled to PBL. We also compare the z_{PBL} provided by the Weather Research and Forecasting (WRF) numerical weather prediction model with respect to the z_{PBL} determined with POLARIS and the MWR under Saharan dust events. WRF underestimates the z_{PBL} during daytime but agrees with the MWR during night-time. The z_{PBL} provided by WRF shows a better temporal evolution compared with the MWR during day-time than at night.

1 Introduction

The planetary boundary layer (PBL) is the region of the troposphere directly influenced by the processes at the Earth's surface. This region typically responds to surface forcing mechanisms with a time scale of about one hour or less (Stull, 1988). The PBL height z_{PBL} is a relevant meteorological variable with a strong effect on air pollution as it defines the atmospheric volume that can be used for pollutant dispersion. Along the time, different approaches based on the use of elastic lidar data have been proposed for detecting the z_{PBL} (e.g., Morille et al., 2007; Granados-Muñoz et al., 2012; Wang et al., 2012; Pal et al., 2013; Coen et al., 2014; Banks et al., 2015). Among them, some methods like the wavelet covariance transform (WCT) have already demonstrated to be a good tool for an automatic and unsupervised detection of the z_{PBL} (Morille et al., 2007; Baars et al., 2008;

Pal et al., 2010;Granados-Muñoz et al., 2012; Wang et al., 2012). This method can be considered the combination of applying the so-called gradient method to a range corrected profile after smoothing by a low-pass filter (Comerón et al., 2013). In these methods, the top of the PBL is associated to the height where there is a sharp decrease of the range corrected signal (RCS) and thus of the aerosol load. Lidars provide an interesting tool for the retrieval of the PBL height, due to their vertical and temporal resolution that allows a continuous monitoring of the PBL. In addition, the number of active ceilometers in Europe has considerably increased due to the low cost and the easy maintenance, allowing us to improve the spatial and temporal monitoring of the PBL. Both lidars and ceilometers use aerosol as a tracer for the identification of the PBL height. This represents a challenge due to the PBL evolution and complex internal structure. The diurnal period is characterized by a mixing layer (statically unstable) where turbulent mixing controls the vertical dispersion up to the top of the convective cells (Seibert, 2000). The mixing boundary layer becomes mixed layer, when the homogenization is complete (neutral stability), something that happens when turbulence is really vigorous and there is an intense convection. During night-time, the stable boundary layer (also known as nocturnal boundary layer) is in direct contact with the surface, and the residual layer is located above the stable layer, loaded with the aerosol that reached high elevation in the previous day (Stull, 1988). The PBL structure is especially complex during the sunrise and sunset when the mixing and residual layers coexist. Furthermore, the coupling of advected aerosol layers in the Free Troposphere with aerosol in the PBL or the presence of clouds lead to under- or overestimation of the PBL height (Granados-Muñoz et al., 2012; Summa et al., 2013).

In this work, we present a new method, called POLARIS (PBL height estimatiOn based on Lidar depolARISation), which is an ameliorated version of the method presented by Baars et al., (2008) and Granados-Muñoz et al., (2012). POLARIS uses the combination of the WCT applied to the RCS and the perpendicular-to-parallel signal ratio (δ) profiles. Using these profiles, different candidates for the z_{PBL} are chosen and the optimum candidate is selected using POLARIS algorithm. POLARIS is particularly useful when advected aerosol layers in the free troposphere are coupled to the PBL because the lidar depolarization ratio profiles provide information about the particle shape allowing the discrimination among different aerosol types. Furthermore, POLARIS improves the z_{PBL} detection since the computation of δ (based on the ratio of two lidar signals) partially cancels out the incomplete overlap effect, allowing the z_{PBL} detection at lower heights than using methods based exclusively on the RCS (affected by incomplete overlap).

Data sets of lidar and microwave radiometer measurements registered in ChArMEx (Chemistry-Aerosol Mediterranean Experiment, http://charmex.lsce.ipsl.fr/) experimental campaigns during the summers of 2012 and 2013 are used in this study for the POLARIS evaluation. ChArMEx is a collaborative research program federating international activities to investigate Mediterranean regional chemistry-climate interactions (Mallet et al., 2016). One of the goals of ChArMEx is to reach a better knowledge on the atmospheric aerosol over the Mediterranean Basin (Dulac et al., 2014; Sicard et al., 2016; Granados-Muñoz et al., 2016). This work contributes to the Mediterranean studies since POLARIS improves the PBL detection under the frequent dust outbreaks affecting this region.

Since the experimental detection of z_{PBL} is spatially and temporally limited due to instrumental coverage, the use of Numerical Weather Prediction (NWP) models for the estimation of z_{PBL} is a feasible alternative. In this regard, several validation studies of these model estimations have been conducted based on lidar and surface and upper air measurements (Dandou et al., 2009; Helmis et al, 2012), some of them in areas close to the study region (Borge et al., 2008; Banks et al., 2015). Results showed that NWP estimations of the z_{PBL} (z_{PBL}^{WRF}) are feasible, but with a tendency to the underestimation of the z_{PBL} in most synoptic conditions. In this study, z_{PBL}^{WRF} is tested against the z_{PBL} derived from POLARIS and MWR measurements under Saharan dust events.

2 Experimental site and instrumentation

In this work we use measurements registered in the Andalusian Institute for Earth System Research (IISTA-CEAMA). This center is located at Granada, in Southeastern Spain (Granada, 37.16°N, 3.61°W, 680 m asl). The metropolitan Granada's population is around 350 000 inhabitants: 240 000 inhabitants from the city and 110 000 inhabitants from the main villages surround the city (www.ine.es). It is a non-industrialized city surrounded by mountains (altitudes up to 3479 m asl, Mulhacén peak). Granada's meteorological conditions are characterized by a large seasonal temperature range (cool winters and hot summers) and by a rainy period between late autumn and early spring with scarce rain the rest of the year.

The main local sources of aerosol particles are the road traffic, the soil re-suspension (during warm-dry season) and the domestic heating based on fuel oil combustion (during winter) (Titos et al., 2012). Additionally, due to its proximity to the African continent, Granada's region is frequently affected by outbreaks of Saharan air masses becoming an exceptional place to characterize Saharan dust. Additionally, Lyamani et al. (2010) and Valenzuela et al. (2012) point to the Mediterranean basin as an additional source of aerosol particles in the region.

MULHACEN is a multiwavelength lidar system with a pulsed Nd:YAG laser, frequency doubled and tripled by Potassium Dideuterium Phosphate crystals. MULHACEN emits at 355, 532 and 1064 nm (output energies per pulse of 60, 65 and 110 mJ, respectively) and registers elastic channels at 355, 532 and 1064 nm and Raman-shifted channels at 387 (from N2), 408 (from H2O) and 607 (from N2) nm. The depolarization measurements are performed by splitting the 532 nm signal by means of a polarizing beam-splitter cube (PBC), being the parallel signal with respect to the polarizing plane of the outgoing laser beam measured in the reflected part of the PBC. The depolarization calibration is performed by means of the ±45◦ calibration method (Freudenthaler et al., 2009). This calibration procedure performed with MULHACEN is described in detail by Bravo-Aranda, et al. (2010) and its systematic errors analysed by Bravo-Aranda, et al. (2016).

The optical path of the parallel and perpendicular channels at 532 nm are designed to be identical up to the PBC where the 532 nm signal is split into parallel and perpendicular before reaching the PMT. This setup allows us to assume almost the same overlap for both polarizing components. Thus, the depolarization profile is practically not influenced by the incomplete overlap since it is cancelled out by the ratio of the perpendicular and parallel channels. Only the thermal dilation and contraction of the lidar optics after the PBC might independently change the overlap function of each channel. Since MULHACEN is deployed inside an air-conditioned building, the temperature fluctuation is small and thus, the overlap difference between the channels might be low. Therefore, we assume significant differences only for small values of the overlap function. Navas-Guzman et al. (2011) and Rogelj et al. (2014) retrieve the overlap function of the total signal at 532 nm (sum of parallel and perpendicular channels) by means of the method presented by Wandinger et al. (2000). This study shows that the full-overlap height of MULHACEN is around 0.72 km agl. Assuming that the artefacts due to thermal fluctuations are negligible for overlap-function values above 70%, depolarization profiles can be exploited in terms of MLH detection above ~0.25 km agl. Further details about the technical specifications of MULHACEN are provided by Guerrero-Rascado et al. (2008, 2009).

A ground-based passive microwave radiometer (RPG-HATPRO, Radiometer Physics GmbH) continuously measured tropospheric temperature and humidity profiles during the studied period. The microwave radiometer (MWR) uses direct detection receivers within two bands: 22-31 GHz (providing information about the tropospheric water vapour profile) and 51-58 GHz (related to the temperature profile). Temperature profiles are retrieved from surface meteorological and the brightness temperature measured at the V-band frequencies with a radiometric resolution between 0.3 and 0.4 K root mean square error at 1-s integration time. The frequencies 51.26, 52.28 and 53.86 GHz are used only in zenith pointing and the frequencies 54.94, 56.66, 57.3 and 58 GHz are considered for all the elevation angles (Meunier et al., 2013). The inversion algorithm is based on neural networks (Rose et al., 2005) trained using the radiosonde database of the Murcia WMO station nr. 08430 located at 250 km from Granada. The accuracy of the temperature profiles is 0.8 K within the first 2 km and 1.5 K between 2 and 4 km. The altitude grid of the inversion increases with height: 30 m below 300 m agl, 50 m between 300-1200 m agl, 200 m between

1200 and 5000 m agl and 400 m above (Navas-Guzmán, 2014). The MWR temperature profile is used to locate the z_{PBL} (z_{PBL}^{MWR}) by two algorithms. Under convective conditions, fuelled by solar irradiance absorption at the surface and the associated heating, the parcel method is used to determine the mixing layer height z_{ML}^{MWR} (Holzworth, 1964). Granados-Muñoz et al. (2012) already validated this methodology obtaining a good agreement with radiosonde measurements. Since the parcel method is strongly sensitive to the surface temperature (Collaud-Coen et al., 2014), surface temperature data provided by the MWR are replaced by more accurate temperature data from a collocated meteorological station, in order to minimize the uncertainties in z_{ML}^{MWR} estimation. Conversely, under stable situations, the stable layer height z_{SL}^{MWR} is obtained from the first point where the gradient of potential temperature (θ) equals zero. Collaud-Coen et al. (2014) determine the uncertainties of the PBL height for both methods by varying the surface temperature by ±0.5°. The uncertainties are on the order of ±50 to ±150 m for the PBL maximum height reached in the early afternoon, although uncertainties up to ±500 m can be found just before sunset. Further details about both methods are given by Collaud-Coen et al. (2014).

3 The POLARIS method

3.1Wavelet Covariance Transform

The wavelet covariance transform $W_F(a,b)$ applied to a generic function of height, $F(z)$, (e.g., RCS or δ) is defined as follows:

$$W_F(a,b) = \frac{1}{a}\int_{z_b}^{z_t} F(z)h\left(\frac{(z-b)}{a}\right)dz \quad \text{Eq. 1}$$

where z is the height, z_b and z_t are the integral limits and $h((z-b)/a)$ is the Haar's function defined by the dilation, a, and the translation, b (Fig. 1).

Fig. 2 shows an example of the WCT applied to the RCS (W_{RCS}). W_{RCS} presents a maximum in coincidence with the sharpest decrease of the RCS and thus, the W_{RCS} maximum is associated to a sharp decrease of the aerosol load which could be related to the top of the PBL. In this sense, Baars et al. (2008) proposed the use of the first maximum in the W_{RCS} profile from surface larger than a threshold value to detect the z_{PBL}. Granados-Muñoz et al. (2012) improved this method using an iterative procedure over the dilation parameter starting at 0.05 km and decreasing with steps of 0.005 km. These studies show that the automatic application of this method provides reliable results of the PBL height in most cases. However, Granados-Muñoz et al. (2012) state that the method tends to fail under more complex scenarios as the aerosol stratification within the PBL or the coupling of aerosol layers with the PBL. To improve the PBL height retrieval for these more complex situations, we introduce the use of the depolarization measurements by means of the POLARIS algorithm described in the next section.

3.2Description of POLARIS

POLARIS is based on the detection of the sharp decrease of the aerosol load with height using the range corrected signal and on the relative changes in the aerosol particle shape with height using the perpendicular-to-parallel signal ratio (δ): low δ values might related to spherical particle shape and vice versa (Gross et al., 2011). Since POLARIS is based on vertical relative changes, the depolarization calibration is not required facilitating the procedure. POLARIS uses 10-min averaged range corrected signal (RCS) and perpendicular-to-parallel signal ratio (δ) and carries out the following steps:

1) The WCT is applied to the RCS and to δ (W_{RCS} and W_δ, respectively). Then, W_{RCS} (W_δ) signal is normalized to the maximum value of RCS (δ) in the first one (two) kilometer(s) above the surface.
2) Three z_{PBL} candidates are determined:

i) C_{RCS}: the height of the W_{RCS} maximum closest to the surface exceeding a certain threshold η_{RCS} (dimensionless). This threshold is iteratively decreased, starting in 0.05, until C_{RCS} is found (Granados-Muñoz et al., 2012). A dilation value (a_{RCS}) of 0.03 km is used according to Granados-Muñoz et al. (2012).

ii) C_{min}: the height of the W_δ minimum closest to the surface exceeding the threshold η_{min} (dimensionless). This threshold is iteratively increased, starting in -0.05, until C_{min} is found. C_{min} indicates the height of the strongest increase of δ.

iii) C_{max}: the height of the W_δ maximum closest to the surface exceeding the threshold η_{max} (dimensionless). This threshold is iteratively decreased, starting in 0.05, until C_{min} is found. C_{max} indicates the height of the strongest decrease of δ.

3) The z_{PBL} attribution is performed comparing the relative location of the candidates since we have experimentally found that each distribution in height of the candidates (e.g, C_{max}>C_{min}>C_{RCS}; C_{min}>C_{max} >C_{RCS}) can be linked with an atmospheric situation as schematized in the flow chart (Fig. 3) and explained below:

a. Only one candidate is found: the z_{PBL} corresponds to the found candidate.

b. Only two candidates are found: the z_{PBL} corresponds to the minimum of the found candidates (Fig. 3 case A). An example is shown in Fig. 4 case A.

c. The three candidates are found: in this case, the attribution of the z_{PBL} has two well-differentiated ways:

c.1. Two matching candidates (C_{RCS}=C_{max} or C_{CRS}=C_{min}): it is considered that C_{CRS} matches C_{max} or C_{min} when the distance between them is less than 150 m. In these cases, the highest (in altitude) of the matching candidates is discarded, leaving only two candidates. Then, we define two layers: from 120 m agl up to the lowest candidate, and the layer between the lowest and the highest candidate. Then, we retrieve the averages ($\bar{\delta}_{C_{RCS}}$ and $\bar{\delta}_\delta$ in Fig. 3) and the variances of δ of the both layers. When the absolute difference between the average value of δ is lower than a threshold δ_t and the variances differ less than 30%, the aerosol type in both layers are considered equal indicating that mixing processes evolve up to the highest candidate. Thus, the z_{PBL} is attributed to the maximum of the two candidates (Fig. 3 and 4 case B or D). Conversely, the aerosol types in both layers are considered different indicating that there is not mixing between the layers and thus, the lowest candidate is the z_{PBL} (Fig. 3 and 4 case C or E).

c.2. No match among the candidates: this situation indicates that the sharpest decrease of the RCS does not coincide with the sharpest decrease/increase of the δ.

c.2.1. C_{max}>C_{min}>C_{RCS}: this situation is experimentally linked to either an aerosol layer coupled to the PBL (both layers are in contact) or a lofted aerosol layer (aerosol layer above the PBL) within the free troposphere. In the case of aerosol layer coupled to the PBL, C_{max} is the top of the coupled layer (i.e., C_{max} is not the z_{PBL}); C_{min} is the limit between the PBL and the coupled layer; and C_{RCS} is an edge of an internal structure within the PBL. In the case of lofted aerosol layer, C_{max} and C_{min} are the top and the base of a lofted layer, respectively whereas C_{RCS} is the z_{PBL}. To differentiate the two situations, we search a local minimum of the W_{RCS} around C_{min} (i.e., $min\left(W_{RCS}(C_{min} \pm 50\ m)\right)$ larger than η_{RCS}^{min}, dimensionless) since the bottom of a lofted layer would also show an increase of the RCS at the same altitude that δ increases (C_{min}). If found, it is confirmed that C_{min} is the bottom of a lofted layer and thus, the z_{PBL} corresponds to C_{RCS} (Fig. 3 and 4 case F). Otherwise, C_{min} detects the z_{PBL} (Fig. 3 and 4 case G).

c.2.2. C_{min}>C_{max}>C_{RCS}: this situation indicates that first RCS decreases, then δ decreases, and finally δ increases. This situation is linked to a multi-layered PBL. In this case, the attribution of the z_{PBL} is performed considering the altitude at which both RCS and δ profiles have the sharpest decrease. To this aim, Σ_{max} and Σ_{RCS} are defined as

$$\Sigma_{\max} = W_\delta(C_{max}) + max\left(W_{RCS}(C_{max} \pm 50\,m)\right) \quad \text{Eq. 2}$$

$$\Sigma_{\mathrm{RCS}} = W_{RCS}(C_{RCS}) + max\left(W_\delta(C_{RCS} \pm 50\,m)\right) \quad \text{Eq. 3}$$

where $max\left(W_{RCS}(C_{max} \pm 50\,m)\right)$ is the maximum of W_{RCS} in the range $C_{max} \pm 50\,m$ and $max\left(W_\delta(C_{RCS} \pm 50\,m)\right)$ is the maximum of W_δ in the range $C_{RCS} \pm 50\,m$. Physically, the parameters $\Sigma_{\max}$ and Σ_{RCS} are the sum of the WCT where both RCS and δ profiles have a sharp decrease. Then, if $\Sigma_{\max} > \Sigma_{\mathrm{RCS}}$, both RCS and δ present a stronger at C_{max} than at C_{RCS} and thus, the z_{PBL} is attributed to C_{max} (Fig. 3 and 4 case J), otherwise the z_{PBL} is attributed to C_{RCS} (Fig. 3 and 4 case I).

c.2.3. In the rest of height distributions of C_{min}, C_{max} and C_{RCS} not considered in b.2.1 and b.2.2, the z_{PBL} is attributed to the minimum of the candidates (C_{min} and C_{max}) (e.g., Fig. 3 and 4 case H).

Finally, the temporal coherence of the z_{PBL} is checked as proposed by Angelini et al. (2009) and Wang et al. (2012). Once z_{PBL} is determined for a certain period, each z_{PBL} is compared with their previous and subsequent values. Those z_{PBL}^{POL} which differ more than 300 m with respect to their previous and subsequent values are considered unrealistic and thus, replaced by the average value of its three or six previous and latter values if available. In this way we guarantee the smoothness of the temporal series of the z_{PBL}. According to Angelini et al. (2009), occasional aerosol stratification may occur within the mixing layer. This type of stratification which are usually short in time are not really linked with the planetary boundary development leading a false detections of the PBL height. A 7-bin moving median filter is used to reject the possible attributions related to this type of aerosol stratification.

To illustrate how the distribution in height of the candidates is related to a specific atmospheric situation, we analyse a particular case at 21:30 UTC on 16 June 2013 (Fig. 5) corresponding to an example of the c.1 scenario. As can be seen, C_{RCS} and C_{max} are located at 4.46 and 4.41 km agl whereas C_{min} is located at 0.7 km agl. Since the different between C_{RCS} and C_{max} is lower than 0.15 km, we assume that both candidates points to the same edge of the layer and thus, this situation corresponds to $C_{RCS} = C_{max} > C_{min}$. The mean and variance of δ in the layer below C_{min} and the layer between C_{min} and C_{max} are 0.65 and $7 \cdot 10^{-4}$ and 0.99 and $91 \cdot 10^{-4}$, respectively. Since the δ mean difference is larger than δ_t and the variances differ more than 30%, we determine that there are two different layers: the PBL (low δ) and the coupled layer (high δ) where $C_{RCS} = C_{max}$ indicates the coupled layer top and C_{min} indicates the limit between the residual and the coupled layer, being chosen as z_{PBL}. In this particular case, POLARIS improves the z_{PBL} detection from 4.46 agl to 0.7 km agl.

3.3 POLARIS adjustment

Fig. 6 shows the time series of the RCS and δ at 532 nm for the 36-hour lidar measurement (10:00 UTC 16 – 19:30 UTC 17 June) of ChArMEx 2013 campaign, the C_{RCS}, C_{max} and C_{min} candidates and the z_{PBL}^{POL} and z_{PBL}^{MWR}. This measurement is used to optimize the algorithm, optimizing the dilation a_δ and the different thresholds (η_{RCS}^{min}, and δ_t). Following a similar procedure as that explained in Granados-Muñoz et al. (2012), different combinations of dilation and threshold values are used to compute z_{PBL}^{POL}. Low dilation values (e.g., <0.2 km) provide wrong PBL detection since the WCT identifies as edge changes in the signal that are related to the noise of the δ profile whereas large dilation values (e.g., >0.5 km) detect only strong edges (e.g., the top of the dust layer). The optimal dilation (a_δ) is established at 0.45 km. This a_δ value is larger than the dilation for the RCS profile (0.3 km) determined by Granados-Muñoz et al. (2012) which may be due to the fact δ is noisier than RCS. In the case of η_{RCS}^{min}, the threshold used to distinguish decoupled layers, a value of 0.01 is chosen considering the signal-to-noise ratio of the RCS in the first kilometer of the atmospheric column. A δ_t value (used in the case b.1 for distinguishing two aerosol layers) of 0.06 is determined since lower values separate the same aerosol layer with slight internal variations and larger values difficult the differentiation between the mixing and residual layer with similar δ values.

During this optimization process z_{PBL}^{MWR} is used as reference. The goal is to minimize the differences between z_{PBL}^{MWR} and z_{PBL}^{POL}, even though discrepancies are still expected between both methodologies due to the use of different tracers (temperature for the MWR and aerosol for POLARIS) and the uncertainties associated to both methods.

The z_{PBL}^{POL} determined with the optimal values of a_δ, η_{RCS}^{min}, and δ_t is shown in Fig. 6. During night-time (from 20:30 UTC on 16 June to 04:00 UTC 17 June), we compare the residual layer height determined by the method which uses only the RCS (C_{RCS}) and by POLARIS (z_{RL}^{POL}) and the stable layer height determined with the MWR (z_{SL}^{MWR}). The C_{RCS} candidates are mainly pointing to either the top of the dust layer or internal substructures within the dust layer (Fig. 6). However, POLARIS distinguishes the transition between the residual aerosol layer and the dust layer. In addition, C_{RCS} shows no or little temporal coherency and large discrepancies with z_{SL}^{MWR} as it is evidenced by the means and standard deviations of the C_{RCS} (2.42±1.6 km agl) and of z_{SL}^{MWR} (0.22±0.01 km agl). On the contrary, z_{RL}^{POL} (0.82±0.3 km agl) is more stable with time than C_{RCS} with closer values to z_{SL}^{MWR}, providing more reliable results. The offset of 600 m observed between z_{SL}^{MWR} and z_{RL}^{POL} during the night is mostly due to the fact that z_{RL}^{POL} corresponds to the residual layer and z_{RL}^{MWR} marks the top of the nocturnal stable layer.

On 16 June 2013, the mean and standard deviation of z_{ML}^{POL}, z_{ML}^{MWR} and C_{RCS} during daytime are 2.0±0.3, 2.7±0.4 and 1.5±1.1 km agl, respectively. C_{RCS} mean is more than 1 km lower than z_{ML}^{MWR} because C_{RCS} is most frequently detecting internal structures rather than the top of the PBL. The large standard deviation of the C_{RCS} (1.1 km) is caused by the detections of either the structures within the PBL at around 1.12 km agl or the top of the dust layer at around 3.8 km agl (Fig. 6). On the contrary, z_{ML}^{POL} mean provides a more comparable value with similar standard deviation. These results evidence that the method which uses only the RCS fails when a dust layer is overlaying the PBL. Besides, z_{ML}^{POL} fits better the trend of z_{ML}^{MWR}.

The main differences between z_{ML}^{POL} and z_{ML}^{MWR} are caused by the different basis of each methodology: z_{ML}^{MWR} is determined using the temperature as tracer whereas POLARIS uses the aerosol. For example, on 16 June 2013, z_{ML}^{MWR} increases from 0.8 km to 2.02 km agl between 10:15 and 11:30 UTC whereas z_{ML}^{POL} increases abruptly from 0.52 to 1.82 km agl between 11:20 and 11:30 UTC (i.e., almost one hour later). This is because z_{ML}^{MWR} growths due to the increase of the temperature at surface level during the morning whereas z_{ML}^{POL} increases later, once the convection processes are strong enough to dissipate the boundary between the mixing and the residual layer. Another example of the influence of the tracer is the 1-km bias between z_{ML}^{POL} and z_{ML}^{MWR} between 18:00 and 21:00 UTC on 16 June 2013. During the late afternoon and early night, the temperature at surface level quickly decreases and the atmospheric stability suddenly changes from instable to stable. This pattern is registered by the z_{ML}^{MWR} decreasing from 1.82 km to 0.055 km agl between 18:00 and 18:30 UTC. The increasing atmospheric stability during the late afternoon and early night stops the convection processes and then the mixing layer becomes the residual layer. This change from mixing to residual layer is tracked by the temporal evolution of z_{RL}^{POL} decreasing from 1.92 km to 0.52 km agl between 18:00 and 24:00 UTC. Therefore, there are differences between z_{PBL}^{POL} and z_{PBL}^{MWR} explained in terms of the tracer used for each method that are not related to a wrong attribution of POLARIS.

4 Validation of POLARIS

After the optimization process, POLARIS is applied in an automatic and unsupervised way to the 72-hour lidar measurement performed during the ChArMEx 2012 campaign (between 9 and 12 July 2012). POLARIS is evaluated comparing z_{PBL}^{POL}, with z_{PBL}^{MWR} and C_{RCS}. During this campaign, a Saharan dust outbreak occurred over the Southern Iberian Peninsula. As it can be seen in Fig. 7, δ values are lower close to the surface (mainly local anthropogenic aerosols) in comparison with the lofted aerosol layers (dust aerosol plumes).

The detection of the z_{PBL} by means of the method applied by Granados-Muñoz et al. (2012) (C_{RCS}) shows an erratic trend during the analysed period when the dust layer is coupled to the PBL (Fig. 7). As it can be seen, C_{RCS} sometimes detects either the top of the dust layer, as in the periods 19:30-22:00 UTC on 09/07 and 15:40-16:10 UTC on 11/07 reaching values above 5

km agl or an internal structure within the dust layer (e.g., between 11:50 and 12:20 UTC on 11/07). These estimations are really far from the z_{ML}^{MWR} and thus, they are not linked with the top of the mixing layer. For example, in the period 15:40-16:10 UTC on 11/07, the difference between C_{RCS} and z_{ML}^{MWR} is around 3 km whereas the difference between z_{ML}^{POL} and z_{ML}^{MWR} is around 0.5 km and thus, we can conclude that the estimation performed using POLARIS significantly improves the detection of the z_{PBL} when an aerosol layer is coupled to the PBL. POLARIS and the method applied by Granados-Muñoz et al. (2012) (C_{RCS}) agree with discrepancies lower than 250 m when the dust layer is decoupled of the PBL (e.g., 00:00-08:00 UTC 10 July, 00:00-09:00 UTC 11 July and 18:00 11 July - 04:45 UTC 12 July) evidencing that the use of POLARIS is also appropriate when no coupled layers are present.

The comparison between z_{ML}^{POL} and z_{ML}^{MWR} shows a good agreement when the mixing layer is well developed (13:00-16:00 UTC on each day). However, some discrepancies are found (e.g., 14:46 UTC 10 July 2012 and 15:51 UTC 11 July 2012). These differences can be easily explained considering the different uncertainties and tracers of both methods, which have different responses during the changing conditions, e.g. those observed during sunset or sunrise. During night-time (e.g. 20 UTC 9 July), the offset between the residual and stable layer can be easily tracked with z_{RL}^{POL} and z_{SL}^{MWR}. POLARIS detects the residual layer instead of the stable layer because the WCT can be applied only from $a_\delta/2$ meters above the first valid value of the profile (~0.25 km agl), i.e., around ~450 m, whereas the z_{SL}^{MWR} is between 100 and 300 m agl.

5. WRF validation using POLARIS and MWR

Recent studies use the z_{PBL} determined using lidar data to validate the z_{PBL} obtained from WRF model (z_{PBL}^{WRF}) (Xie et al., 2012; Pichelli et al., 2014 and Banks et al., 2015). In this section, we take the advantage of the z_{PBL} determined by POLARIS (z_{PBL}^{POL}) together with the microwave radiometer z_{PBL}^{MWR} during CHArMEx 2012 and 2013 to validate the z_{PBL}^{WRF}.

5.1 WRF model setup

The model configuration consists of four nested domains with 27, 9, 3 and 1 km (approximately) spatial resolution domains, respectively, and 50 vertical levels. The outputs (i.e., temperature, wind, and humidity profiles, etc.) of the 1-km domain are analysed. The initial and boundary conditions for the WRF model runs are taken from the NCEP High Resolution Global Forecast System data set (www.emc.ncep.noaa.gov) every 6 hours.

The choice of the model physical parameterization is based on the results of previous evaluation studies conducted in the study area (Arbizu-Barrena et al., 2015). Particularly, the Mellor-Yamada Nakanishi and Niino Level 2.5 is selected for the PBL parameterization (Nakanishi and Niino, 2009). The parameterizations used for the rest of physical schemes are: the Eta (Ferrier) microphysics parameterization scheme (Rogers et al., 2005), the RRTM long-wave radiation parameterization (Mlawer et al., 1997), the Dudhia scheme for short-wave radiation parameterization (Dudhia, 1989), the 5-layer thermal diffusion land surface parameterization (Dudhia, 1996) and, for coarser domains, the Kain-Fritsch (new Eta) cumulus parameterization (Kain, 2004).

5.2 Comparison of the PBL heights determined by WRF, POLARIS and microwave radiometer

Fig. 6 and 7 show the temporal evolution of the PBL heights determined by means of POLARIS (z_{PBL}^{POL}), the MWR (z_{PBL}^{MWR}) and WRF (z_{PBL}^{WRF}) during the ChArMEx campaign on 2012 (09:00 UTC 16 June– 20:00 UTC 17 June) and 2013 (12:00 UTC 9 July – 06:00 12 July).

During daytime on both campaigns, WRF underestimates the z_{PBL} (lower values) with respect to z_{PBL}^{POL} and z_{PBL}^{MWR} in agreement with the study presented by Banks et al. (2015) and Banks and Baldasano (2016). For example, z_{PBL}^{WRF} is 1 km below z_{PBL}^{POL} and z_{PBL}^{MWR} on 16/06 2013 (Fig. 6) and on 9 and 10 July 2012 (Fig. 7). Nevertheless, the z_{PBL} time series of all methods show similar

patterns. Table 1 shows the determination coefficient R^2 and the mean of the differences (i.e., bias) among z_{PBL}^{WRF}, z_{PBL}^{POL} and z_{PBL}^{MWR} during night- and day-time.

During free-cloud day-time, the correlation between z_{PBL}^{WRF} and z_{PBL}^{POL} can be well differentiated. $R_{POL-WRF}^2$ is larger on 10 and 11 July 2012 than on 9 July 2012 and 16 June 2013. According to the time series of the δ (Fig. 6 and 7), it can be seen that the coupling of the dust layer to the PBL is stronger on 10 and 11 July 2012 than on 9 July 2012 and 16 June 2013. Additionally, the mean of bias values between POLARIS and WRF ($\overline{\Delta_{PBL}^{POL-WRF}}$), larger than 800 meters, points to the aforementioned underestimation of the convective processes. At this regard, several possibilities are feasible: (i) too stringent conditions for the WRF parameterization, which can influence directly the results (Xie et al., 2012; Banks et al., 2015); (ii) insufficient number of the WRF model vertical levels within the PBL limits; (iii) the different definitions of the PBL applied to each method, and (iv) the presence of Saharan dust layer (Fig. 6 and 7). Among these causes, the (i) and (ii) should affect to the whole period, not only the periods with the strongest coupling of the dust layer to the PBL. In addition, the different definitions of PBL seem difficult to give rise to such a large bias. In fact, POLARIS and the parcel method use different tracers (e.g., temperature and aerosol) but they generally show better agreement than WRF. Thus, the more plausible cause is the inability of the used WRF PBL parameterization to account properly for this particular kind of events.

The correlations between MWR and WRF ($R_{MWR-WRF}^2$) are between 0.395 and 0.664 during free-cloud day-time without a clear dependence with the presence or the coupling of the dust layer. The lowest $R_{MWR-WRF}^2$ and the largest $\overline{\Delta_{PBL}^{MWR-WRF}}$ ocurs on 16 June in coincidence with the lowest $R_{POL-WRF}^2$. On this day, the WRF model estimates that the convective processes start at 13:35 and ends at 16:15 UTC, whereas MWR detects convective processes between 10:30 and 18:00 UTC (i.e., 5 hours difference). The good agreement between POLARIS and MWR ($R_{POL-MWR}^2$ = 0.803) indicates that the main cause of the differences in the PBL height is the short duration of the convective processes estimated by the WRF model.

During night-time, z_{PBL}^{WRF} and z_{PBL}^{MWR} agree, with differences below 0.38 km (see Table 1). However, a low temporal correlation is observed ($R_{MWR-WRF}^2$ values between 0.032 and 0.364), showing the opposite behaviour observed during daytime. The large $\overline{\Delta_{PBL}^{POL-WRF}}$ and $\overline{\Delta_{PBL}^{POL-MWR}}$ values evidence that POLARIS detects the residual layer whereas MWR and WRF detect the top of the stable layer. Despite POLARIS and WRF are detecting different layers, we find a larger correlation among them ($R_{POL-WRF}^2$) than between MWR and WRF ($R_{MWR-WRF}^2$).

Finally, the lowest $R_{POL-WRF}^2$ coincides with the lowest $\overline{\Delta_{PBL}^{POL-WRF}}$ and $\overline{\Delta_{PBL}^{MWR-WRF}}$ values on 17 June. The presence of clouds from midday (cloud base at 9.32 km agl) until the end of the measurements (cloud base at 1.32 km agl) may explain this behaviour since i) the systematic underestimation from WRF might be compensated by the cloudy conditions inhibiting the strength of convective processes and ii) the track of the PBL evolution is more difficult to fit during cloudy conditions, considering the different tracers (i.e., aerosol and temperature).

To sum up, during night-time, z_{PBL}^{WRF} and z_{PBL}^{MWR} values agree but more similar temporal evolution is found between WRF and POLARIS. However, during daytime, the WRF model underestimates the z_{PBL}. Since POLARIS allows detecting reliable PBL heights under Saharan dust outbreaks, it might be used for the improvement of the WRF parameterization.

6. Conclusion

The perpendicular-to-parallel signal ratio (i.e., the uncalibrated volume linear depolarization ratio), together with the lidar range corrected signal, are used to develop a new algorithm, called POLARIS, for the detection of the planetary boundary layer height (z_{PBL}). The z_{PBL} provided by POLARIS, z_{PBL}^{POL}, is optimized by comparison with the z_{PBL} derived from microwave radiometer measurements (temperature profiles), z_{PBL}^{MWR}, using continuous 36-hour lidar and MWR measurements. z_{PBL}^{POL} is validated by comparison with the z_{PBL}^{MWR}, using continuous 72-hour lidar and MWR measurements. These measurements were performed during the ChArMEx campaigns conducted in 2012 and 2013. These continuous-term measurements are crucial for the adjustment and validation of POLARIS since they allow the tracking of the evolution of the coupling between advected

aerosol layers and the planetary boundary layer. A better agreement is obtained between POLARIS and the methods applied to the MWR measurements compared with the WCT method exclusively applied to the range corrected signal during complex scenarios (e.g., when a Saharan dust layer is coupled to the PBL). Despite POLARIS is validated using dust layers coupled to the PBL, a priori, it can be used for any layer coupled to the PBL if the aerosol particle-shape is different enough to be detected by the depolarization profile. This is a remarkable improvement compared to previous methods based on the WCT applied to the RCS.

The z_{PBL} is also determined by means of WRF model, z_{PBL}^{WRF}, under Saharan dust outbreaks. During daytime, z_{ML}^{WRF} is considerably lower than z_{ML}^{POL} and z_{ML}^{MWR} with larger differences under coupling-layer situation. However, WRF and MWR provides similar z_{PBL} during night-time although z_{SL}^{WRF} shows a better temporal correlation with z_{RL}^{POL} than with z_{SL}^{MWR}. The comparison between POLARIS and WRF evidences the model difficulties to determine the z_{PBL} when advected layers are coupled to the PBL. Since POLARIS allows the detection of reliable PBL heights under Saharan dust outbreaks, it might be used for the improvement of the WRF parametrization.

This study demonstrates that the depolarization measurement is an interesting proxy for the PBL detection since it provides reliable PBL heights under coupling-layer situation. Moreover, considering the next ceilometer generations with depolarization capabilities, this study will be useful for an automatic and unsupervised PBL detection. At this regard, further investigations will lead to a proper PBL height detection in all atmospheric conditions.

Acknowledgements

This work was supported by the Andalusia Regional Government through project P12-RNM-2409, by the Spanish Ministry of Economy and Competitiveness through projects CGL2013-45410-R and CGL2016-81092-R, and by the European Union's Horizon 2020 research and innovation programme through project ACTRIS-2 (grant agreement No 654109). The authors thankfully acknowledge the FEDER program for the instrumentation used in this work. This work was also partially funded by the University of Granada through the contract "Plan Propio. Programa 9. Convocatoria 2013". The authors express gratitude to the ChArMEx project of the MISTRALS (Mediterranean Integrated Studies at Regional and Local Scales; http://www.mistrals-home.org) multidisciplinary research programme.

References

Angelini, F., Barnaba, F., Landi, T. C., Caporaso, L., and Gobbi, G. P.: Study of atmospheric aerosols and mixing layer by lidar, Radiat. Prot. Dosim., 137(3-4), 275-279, doi: 10.1093/rpd/ncp219, 2009.

Arbizu-Barrena, C., Pozo-Vázquez, D., Ruiz-Arias, J. A., and Tovar-Pescador, J.: Macroscopic cloud properties in the WRF NWP model: An assessment using sky camera and ceilometer data. Journal of Geophysical Research: Atmospheres 120 (19), doi: 10.1002/2015JD023502, 2015.

Baars, H., Ansmann, A., Engelmann, R., and Althausen, D.: Continuous monitoring of the boundary-layer top with lidar. Atmospheric Chemistry and Physics, 8, 7281–7296, doi 10.5194/acp-8-7281-2008, 2008.

Banks, R. F., Tiana-Alsina, J., Rocadenbosch, F., and Baldasano, J. M.: Performance evaluation of the boundary-Layer height from lidar and the Weather Research and Forecasting model at an urban coastal site in the North-East Iberian Peninsula,Boundary-Layer Meteorology, 157(2), 265–292, doi: 10.1007/s10546-015-0056-2, 2015.

Banks, R. F., and Baldasano, J. M.: Impact of WRF model PBL schemes on air quality simulations over Catalonia, Spain. Science of the Total Environment 572 (2016) 98–113, doi:10.1016/j.scitotenv.2016.07.167, 2016.

Borge, R., Alexandrov, V., Vas, J. J. del, Lumbreras, J., and Rodríguez, E.: A comprehensive sensitivity analysis of the WRF model for air quality applications over the Iberian Peninsula. Atmos Environ 42(37), 8560–8574, doi: 10.1016/j.atmosenv.2008.08.032,2008.

Bravo-Aranda, J.A, Navas-Guzmán, F., Guerrero-Rascado, J.L., Pérez-Ramírez, D., Granados-Muñoz, M.J., and Alados-Arboledas, L.: Analysis of lidar depolarization calibration procedure and application to the atmospheric aerosol characterization, International Journal of Remote Sensing 34(9-10), 3543-3560, doi: 10.1080/01431161.2012.716546, 2013.

Bravo-Aranda, J. A., Belegante, L., Freudenthaler, V., Alados-Arboledas, L., Nicolae, D., Granados-Muñoz, M. J., Guerrero-Rascado, J. L., Amodeo, A., D'Amico, G., Engelmann, R., Pappalardo, G., Kokkalis, P., Mamouri, R., Papayannis, A., Navas-Guzmán, F., Olmo, F. J., Wandinger, U., Amato, F., and Haeffelin, M.: Assessment of lidar depolarization uncertainty by means of a polarimetric lidar simulator, Atmos. Meas. Tech., 9, 4935-4953, doi:10.5194/amt-9-4935-2016, 2016.

Cairo, F., Di Donfrancesco, G., Adriani, A., Pulvirenti, L., and Fierli F.: Comparison of various linear depolarization parameters measured by lidar, Appl Optics, 38, 4425-4432, doi: 10.1364/AO.38.0044251999.

Collaud-Coen, M. C., Praz, C., Haefele, A., Ruffieux, D., Kaufmann, P., and Calpini, B.: Determination and climatology of the planetary boundary layer height above the Swiss plateau by in situ and remote sensing measurements as well as by the COSMO-2 model. Atmospheric Chemistry and Physics, 14, 13205–13221, doi: 10.5194/acp-14-13205-2014, 2014.

Comerón, A., Sicard, M., and Rocadenbosch, F.: Wavelet correlation transform method and gradient method to determine aerosol layering from lidar returns: Some comments. Journal of Atmospheric and Oceanic Technology, 30(6), 1189–1193, doi: 10.1175/JTECH-D-12-00233.1, 2013.

Dandou, A., Tombrou, M., Schäfer, K., Emeis, S., Protonotariou, A., Bossioli, D., Soulakellis, N., and Suppan, P.: A Comparison Between Modelled and Measured Mixing-Layer Height Over Munich. Boundary-Layer Meteorol 131:425–440, doi: 10.1007/s10546-009-9373-7, 2009.

Dudhia, J., 1989: Numerical study of convection observed during the Winter Monsoon Experiment using a mesoscale two–dimensional model. J. Atmos. Sci., 46, 3077–3107, doi: 10.1175/1520-0469(1989)046<3077:NSOCOD>2.0.CO;2, 1988.

Dudhia, J., 1996: A multi-layer soil temperature model for MM5. The Sixth PSU/NCAR Mesoscale Model Users' Workshop. Bouilder, CO.

Dulac, F.: An overview of the Chemistry-Aerosol Mediterranean Experiment (ChArMEx), European Geosciences Union General Assembly, Geophysical Research Abstracts Vol. 16, EGU2014-11441, 27 April–2 May 2014, Vienna, Austria, 2014.

Granados-Muñoz, M. J., Navas-Guzmán, F., Bravo-Aranda, J. A., Guerrero-Rascado, J. L., Lyamani, H., Fernández-Gálvez, J., and Alados-Arboledas, L.: Automatic determination of the planetary boundary layer height using lidar: One-year analysis over southeastern Spain. Journal of Geophysical Research: Atmospheres, 117(D18), doi: 10.1029/2012JD017524, 2012.

Granados-Muñoz, M. J., Navas-Guzmán, F., Guerrero-Rascado, J. L., Bravo-Aranda, J. A., Binietoglou, I., Pereira, S. N., Basart, S., Baldasano, J. M., Belegante, L., Chaikovsky, A., Comerón, A., D'Amico, G., Dubovik, O., Ilic, L., Kokkalis, P., Muñoz-Porcar, C., Nickovic, S., Nicolae, D., Olmo, F. J., Papayannis, A., Pappalardo, G., Rodríguez, A., Schepanski, K., Sicard, M., Vukovic, A., Wandinger, U., Dulac, F., and Alados-Arboledas, L.: Profiling of aerosol microphysical properties at several EARLINET/AERONET sites during the July 2012 ChArMEx/EMEP campaign, Atmos. Chem. Phys., 16, 7043-7066, doi:10.5194/acp-16-7043-2016, 2016.

Gross, S., Tesche, M., Freudenthaler, V., Toledano, C., Weigner, M., Ansmann, A., Althausen, D., Seefeldner, M.: Characterization of Saharan dust, marine aerosols and mixtures of biomass-burning aerosols and dust by means of multi-wavelength depolarization and Raman lidar measurements during SAMUM 2. Tellus B, v. 63B, 706–724, doi:10.3402/tellusb.v63i4.16369, 2011.

Guerrero-Rascado, J. L., Ruiz, B., and Alados-Arboledas, L.: Multi-spectral lidar characterization of the vertical structure of Saharan dust aerosol over southern Spain, Atmos. Envion., 42, 2668-2681, doi:10.1016/j.atmosenv.2007.12.062, 2008.

Guerrero-Rascado, J. L., Olmo, F. J., Avilés-Rodríguez, I., Navas-Guzmán, F., Pérez-Ramírez, D., Lyamani, H., and Alados-Arboledas, L.; Extreme Saharan dust event over the southern Iberian Peninsula in September 2007: active and passive remote sensing from surface and satellite, Atmos. Chem. Phys., 9, 8453-8469, doi: 10.5194/acp-9-8453-2009, 2009.

Helmis, C., Tombrou, M., Schäfe., K., Münkel, C., Bossioli, E. & Dandou, A. : A comparative study and evaluation of mixing-height estimation based on Sodar-RASS, ceilometer data and numerical model simulations, Boundary-Layer Meteorology, 145, 507–526, doi: 10.1007/s10546-012-9743-4, 2012.

Holzworth, G. C.: Estimates of mean maximum mixing depths in the contiguous United States. Monthly Weather Review, 92, 235–242, 10.1175/1520-0493(1964)092<0235:EOMMMD>2.3.CO;2, 1964.

Kain, John S., 2004: The Kain–Fritsch convective parameterization: An update. J. Appl. Meteor., 43, 170–181, doi: http://dx.doi.org/10.1175/1520-0450(2004)043<0170:TKCPAU>2.0.CO;2, 2004.

Lyamani, H., Olmo, F. J., & Alados-Arboledas, L. (2010). Physical and optical properties of aerosols over an urban location in Spain: seasonal and diurnal variability. Atmospheric Chemistry and Physics, 10, 239–254, doi: 10.5194/acp-10-239-2010, 2010.

Mallet, M., Dulac, F., Formenti, P., Nabat, P., Sciare, J., Roberts, G., Pelon, J., Ancellet, G., Tanré, D., Parol, F., Denjean, C., Brogniez, G., di Sarra, A., Alados-Arboledas, L., Arndt, J., Auriol, F., Blarel, L., Bourrianne, T., Chazette, P., Chevaillier, S., Claeys, M., D'Anna, B., Derimian, Y., Desboeufs, K., Di Iorio, T., Doussin, J.-F., Durand, P., Féron, A., Freney, E., Gaimoz, C., Goloub, P., Gómez-Amo, J. L., Granados-Muñoz, M. J., Grand, N., Hamonou, E., Jankowiak, I., Jeannot, M., Léon, J.-F., Maillé, M., Mailler, S., Meloni, D., Menut, L., Momboisse, G., Nicolas, J., Podvin, T., Pont, V., Rea, G., Renard, J.-B., Roblou, L., Schepanski, K., Schwarzenboeck, A., Sellegri, K., Sicard, M., Solmon, F., Somot, S., Torres, B., Totems, J., Triquet, S., Verdier, N., Verwaerde, C., Waquet, F., Wenger, J., and Zapf, P.: Overview of the Chemistry-Aerosol Mediterranean Experiment/Aerosol Direct Radiative Forcing on the Mediterranean Climate (ChArMEx/ADRIMED) summer 2013 campaign, Atmos. Chem. Phys., 16, 455-504, doi:10.5194/acp-16-455-2016, 2016.

Meunier, V., Löhnert, U., Kollias, P., and Crewell, S.: Biases caused by the instrument bandwidth and beam width on simulated brightness temperature measurements from scanning microwave radiometers, Atmospheric Measurement Techniques, 6, 1171–1187, doi:10.5194/amt-6-1171-2013,2013.

Milovac, J., Warrach-Sagi, K., Behrendt, A., Späth, F., Ingwersen, J., and Wulfmeyer, V.: Investigation of PBL schemes combining the WRF model simulations with scanning water vapor differential absorption lidar measurements, J. Geophys. Res. Atmos., 121, 624–649, doi:10.1002/2015JD023927, 2016.

Morille, Y., Haeffelin, M., Drobinski, P., and Pelon, J.:STRAT: An Automated Algorithm to Retrieve the Vertical Structure of the Atmosphere from Single-Channel Lidar Data. Journal of Atmospheric and Oceanic Technology, 24(5), 761–775, doi: 10.1175/JTECH2008.1, 2007.

Mlawer, E. J., Taubman, S. J., Brown, P. D., Iacono, M. J., and Clough, S. A.: Radiative transfer for inhomogeneous atmospheres: RRTM, a validated correlated–k model for the longwave. J. Geophys. Res.,102, 16663–16682, doi: 10.1029/97JD00237, 1997.

Nakanishi, M., and Niino, H.: Development of an improved turbulence closure model for the atmospheric boundary layer. J. Meteor. Soc. Japan, 87, 895–912, doi: 10.1029/97JD00237, 2009.

Navas Guzmán, F., Guerrero Rascado, J. L., and Alados Arboledas, L.: Retrieval of the lidar overlap function using Raman signals, Óptica Pura y Aplicada, 44(1), 71-75, 2011.

Navas-Guzmán, F., Fernández-Gálvez, J., Granados-Muñoz, M. J., Guerrero-Rascado, J. L., Bravo-Aranda, J. A., and Alados-Arboledas, L. (2014). Tropospheric water vapour and relative humidity profiles from lidar and microwave radiometry. Atmospheric Measurement Techniques, 7(5), 1201–1211, doi: 10.5194/amt-7-1201-2014, 2014.

Pal, S., Behrendt, A., and Wulfmeyer, V.: Elastic-backscatter-lidar-based characterization of the convective boundary layer and investigation of related statistics. Annales Geophysicae, 28(3), 825–847, doi: 10.5194/angeo-28-825-2010, 2010.

Pichelli, E., Ferretti, R., Cacciani, M., Siani, A. M., Ciardini, V., and Di Iorio, T.:The role of urban boundary layer investigated with high-resolution models and ground-based observations in Rome area: A step towards understanding parameterization potentialities. Atmospheric Measurement Techniques, 7(1), 315–332, doi: 10.5194/amt-7-315-2014, 2014.

Rogelj, N., Guerrero-Rascado, Navas-Guzmán, F., Bravo-Aranda, J. A., Granados-Muñoz, M. J., Alados-Arboledas L.: Experimental determination of UV- and VIS- lidar overlap function. Optica Pura Y Aplicada, 47, 169-175, doi: 10.7149/OPA.47.3.169, 2011.

Rogers, E., Black, T., Ferrier, B., Lin, Y., Parrish, D., and DiegoG.: Changes to the NCEP MesoEta Analysis and Forecast System: Increase in resolution, new cloud microphysics, modified precipitation assimilation, modified 3DVAR Analysis. Available online at www.emc.ncep.noaa.gov/mmb/mmbpll/eta12tpb/), 2005.

Rose, T., Crewell, S., Lohnert, U., and Simmer C.: A network suitable microwave radiometer for operational monitoring of the cloudy atmosphere, Atmos Res, 75(3), 183-200, doi: 10.1016/j.atmosres.2004.12.005, 2005.

Seinfeld, J. H., and S. N. Pandis (1998), Atmospheric chemistry and physics, Wiley-Interscience.

Seibert, P., Beyrich, F., Gryningc, S.-E.,Joffred, S., Rasmussene, A., Tercierf,P.: Review and intercomparison of operational methods for the determination of the mixing height. Atmospheric Environment, 34(7), 1001–1027, doi: 10.1016/S1352-2310(99)00349-0, 2000.

Sicard, M., Barragan, R., Dulac, F., Alados-Arboledas, L., and Mallet, M.: Aerosol optical, microphysical and radiative properties at three regional background insular sites in the western Mediterranean Basin, Atmos. Chem. Phys. Discuss., doi:10.5194/acp-2015-823, in review, 2016.

Skamarock, W. C., Klemp, J. B., Dudhia, J., Gill, D. O., Barker, D. M., Duda, M., Huang, X.-Y., Wang, W. and Powers, J. G.:, A description of the advanced research WRF version 3, NCAR Technical Note, 2008.

Stull, R. B.: An Introduction to Boundary Layer Meteorology, Kluwer Academic Publishers, 1988.

Stull, R. B.: Meteorology: For Scientists and Engineers, Thomson Learning, 2000.

Summa, D., Di Girolamo, P., Stelitano, D., and Cacciani, M.: Characterization of the planetary boundary layer height and structure by Raman lidar: comparison of different approaches. Atmospheric Measurement Techniques, 6(12), 3515–3525,doi: 10.5194/amt-6-3515-2013, 2013.

Titos, G., Foyo-Moreno, I., Lyamani, H., Querol, X., Alastuey, A., and Alados-Arboledas, L.: Optical properties and chemical composition of aerosol particles at an urban location: An estimation of the aerosol mass scattering and absorption efficiencies. Journal of Geophysical Research Atmospheres, 117(4), 1–12,doi: 10.1029/2011JD016671, 2012.

Valenzuela, A., Olmo, F. J., Lyamani, H., Antón, M., Quirantes, A., and Alados-Arboledas, L.: Aerosol radiative forcing during African desert dust events (2005–2010) over Southeastern Spain, Atmos. Chem. Phys., 12, 10331-10351, doi:10.5194/acp-12-10331-2012, 2012.

Wang, Z., Cao, X., Zhang, L., Notholt, J., Zhou, B., Liu, R., and Zhang, B.: Lidar measurement of planetary boundary layer height and comparison with microwave profiling radiometer observation. Atmospheric Measurement Techniques, 5(8), 1965–1972, doi: 10.5194/amt-5-1965-2012, 2012.

Xie, B., Fung, J. C. H., Chan, A., and Lau, A.: Evaluation of nonlocal and local planetary boundary layer schemes in the WRF model. Journal of Geophysical Research Atmospheres, 117(12), 1–26, doi: 10.1029/2011JD017080, 2012.

Table 1: R² among z_{PBL}^{POL}, z_{PBL}^{MWR} and z_{PBL}^{WRF} during ChArMEx 2012 and 2013. Points are the number of values used to retrieve the correlation factor. $\overline{\Delta_{PBL}^{POL-WRF}}$, $\overline{\Delta_{PBL}^{MWR-WRF}}$, and $\overline{\Delta_{PBL}^{POL-MWR}}$ are the mean differences between the z_{PBL}^{POL}, z_{PBL}^{MWR}, and z_{PBL}^{MWR}. Daytime is considered between 06:00 and 19:00 UTC (PBL means the ML) and night-time is the rest of the day (PBL means the RS).

		Daytime	$R^2_{POL-WRF}$	Points	$\overline{\Delta_{PBL}^{POL-WRF}}$(m)	$R^2_{MWR-WRF}$	Points	$\overline{\Delta_{PBL}^{MWR-WRF}}$(m)	$R^2_{POL-MWR}$	Points	$\overline{\Delta_{PBL}^{POL-MWR}}$(m)
ChArMEx	2012	9th July	0.236	12	850	0.664	12	440	0.598	12	380
		10th July	0.763	26	680	0.605	26	410	0.718	26	240
		11th July	0.661	26	1170	0.441	26	520	0.361	26	1700
	2013	16th June	0.122	26	830	0.395	26	1330	0.803	26	570
		17th July	0.018	26	420	0.094	26	280	0.304	26	40
		Night-time	$R^2_{POL-WRF}$	Points	$\overline{\Delta_{PBL}^{POL-WRF}}$(m)	$R^2_{MWR-WRF}$	Points	$\overline{\Delta_{PBL}^{MWR-WRF}}$(m)	$R^2_{POL-MWR}$	Points	$\overline{\Delta_{PBL}^{POL-MWR}}$(m)
	2012	9th July	0.660	28	940	0.364	17	190	0.463	17	1150
		10th July	0.640	28	930	0.032	9	180	0.057	9	1130
		11th July	0.440	28	770	0.230	11	380	0.062	11	1130
	2013	16th June	0.030	28	390	0.099	9	400	0.028	9	730

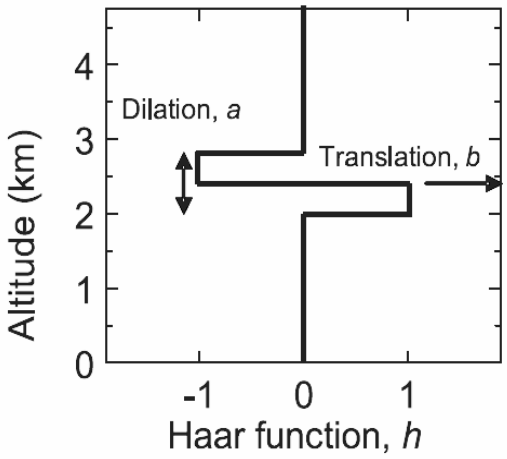

Figure 1: Haar's function defined by the dilation (*a*) and the translation (*b*).

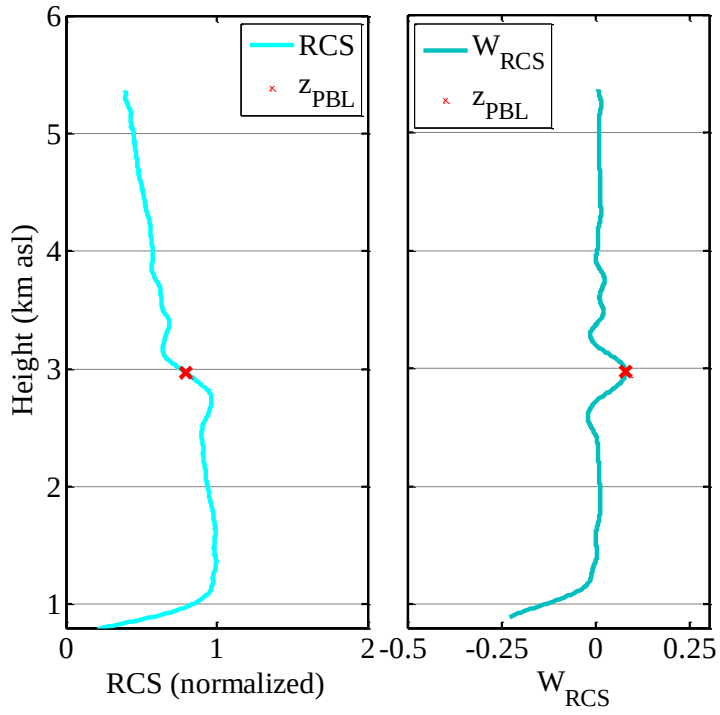

Figure 2: Example of a normalized RCS and its wavelet covariance transform. Red cross indicates the possible location of the PBL height.

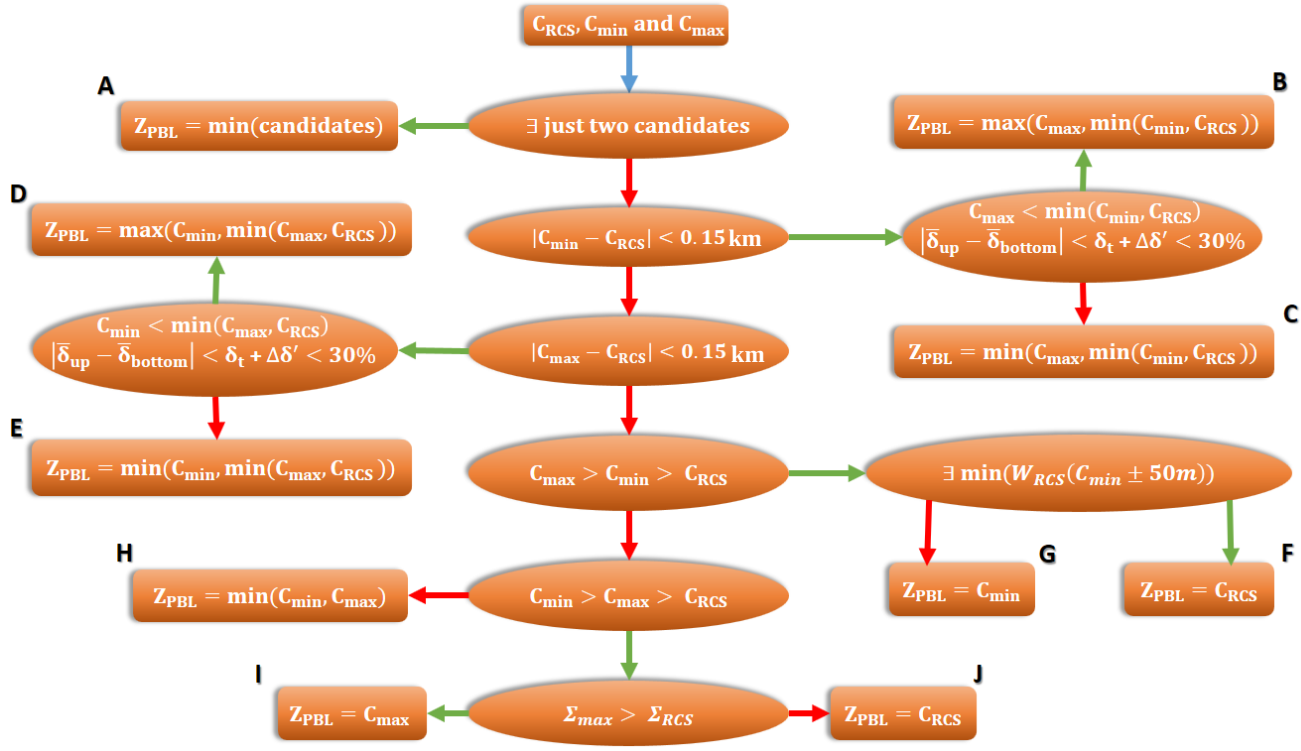

Figure 3: Flux diagram of the algorithm used by POLARIS to determine the z_{PBL}. C_{min}, C_{max} and C_{RCS} are the candidates. The blue arrow indicates the start. Conditions are marked in ellipses and the final attribution of the z_{PBL} in rectangles. The green and red arrows indicate the compliance and noncompliance of the conditions, respectively. The rest of the symbols are explained in the text.

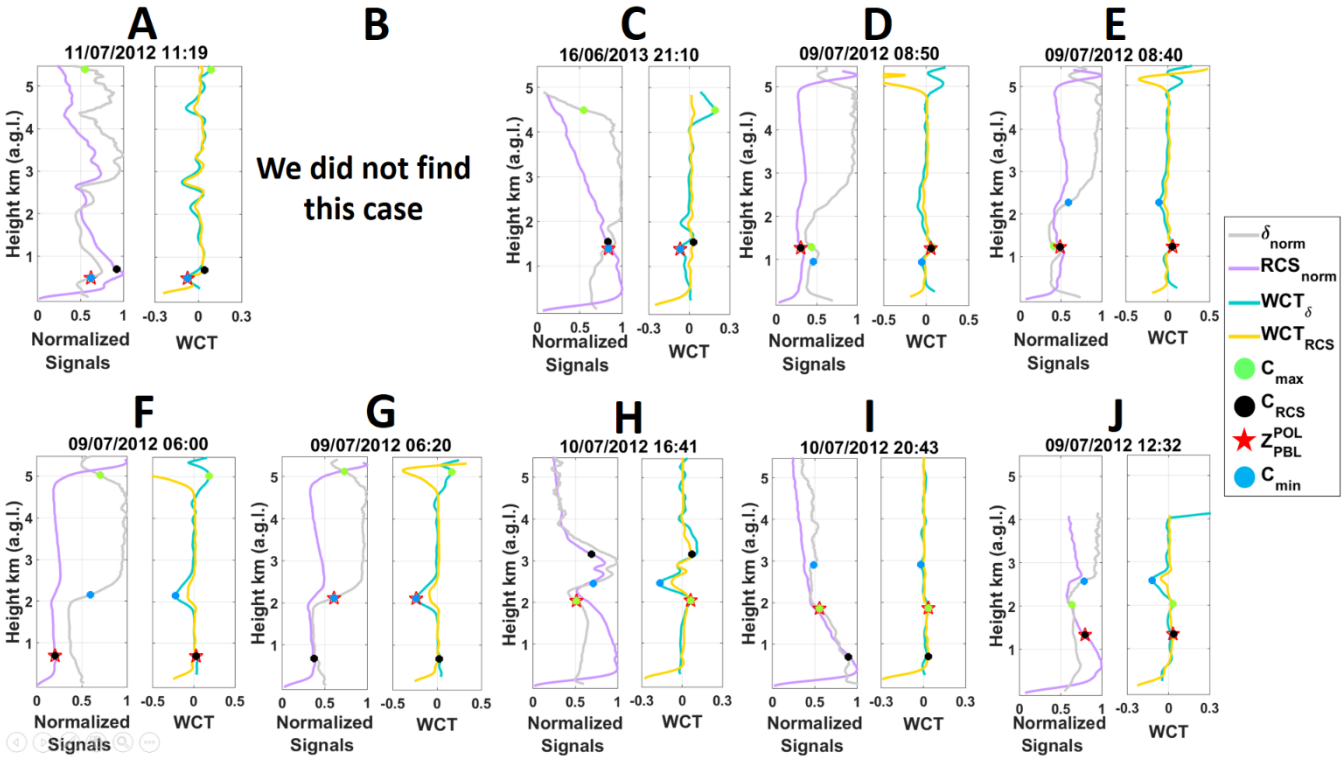

Figure 4: Examples of the cases mentioned in Figure 3 occurred during ChArMEx 2012 and 2013. Normalized RCS (violet line) and δ (grey line) are shown in left axis and WCT of RCS (yellow line) and δ (ligh blue line) are shown in right axis. C_{min} (blue dot), C_{max} (green dot), C_{RCS} (black dot) and the final attribution z^{POL}_{PBL} (red start) are shown in both axis.

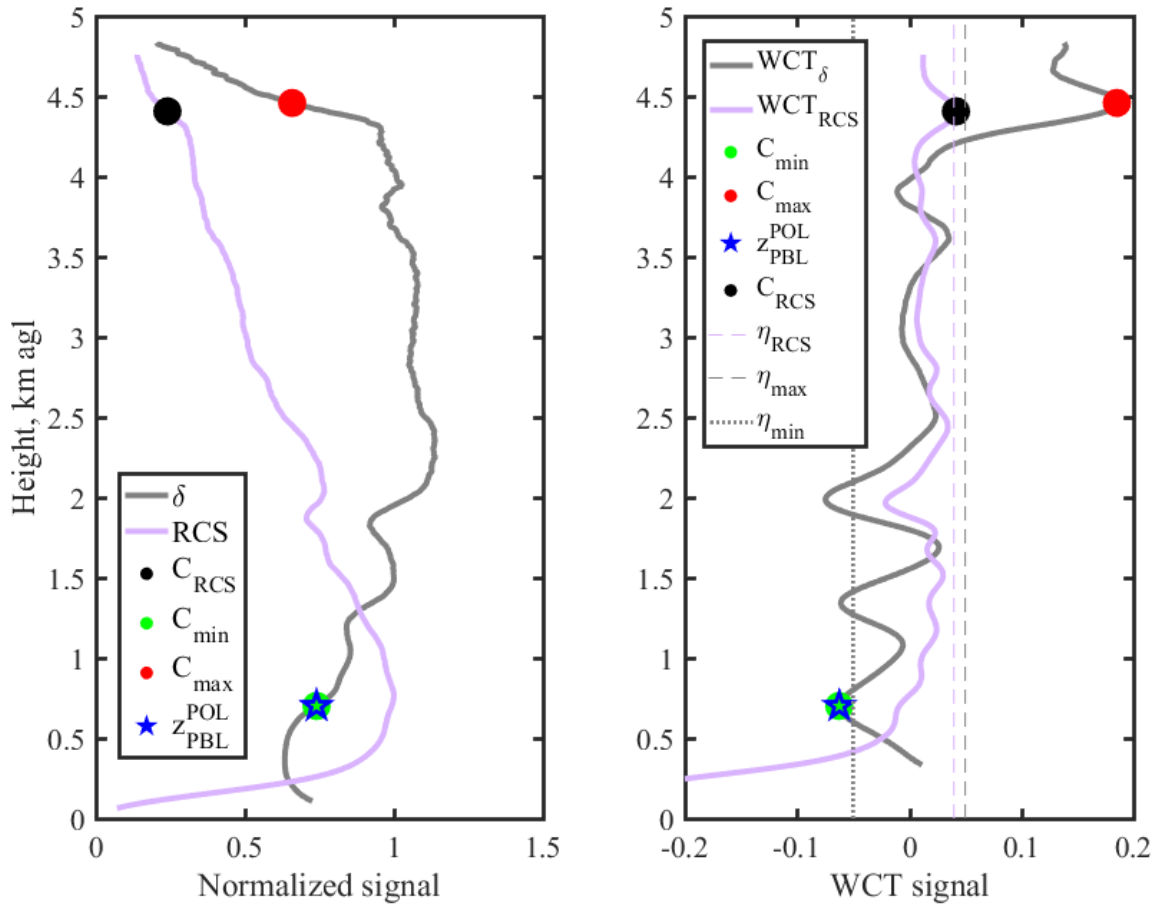

Figure 5: Normalized RCS and δ profiles (left). WCT of the RCS, δ and thresholds η_{min} (–0.05) and η_{RCS} (0.05), η_{max} (0.04) (right) at 21:30 UTC 16 June 2013. C_{CRS}, C_{min} and C_{max} candidates and z_{PBL}^{POL} are shown in both axes.

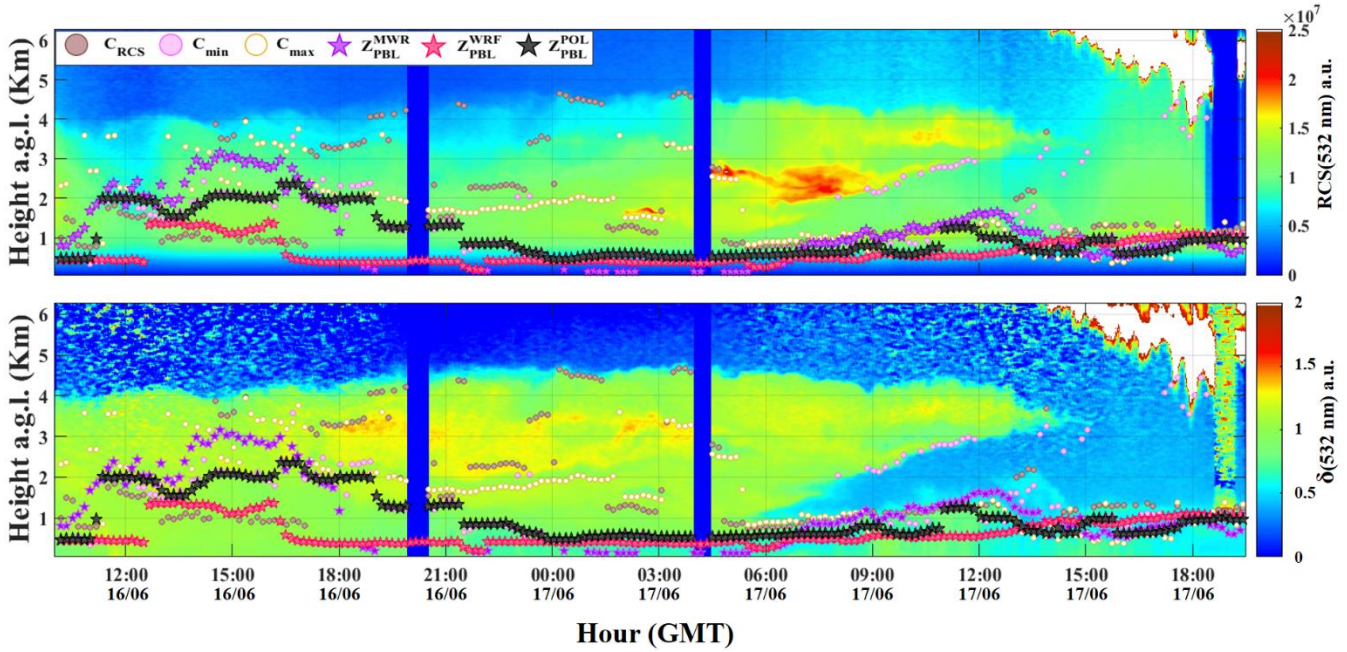

Figure 6: Temporal evolution of the range corrected signal (RCS) (top) and the perpendicular-to-parallel signal ratio (δ) (bottom) in the period 09:00 16 June - 20:00 17 June 2013 (colour maps). The scatter plots represent the candidate for z_{PBL}: C_{RCS} (brown dot), C_{min} (pink dot) and C_{max} (ochre dot). The z_{PBL} determined with POLARIS (black star), by the parcel method using MWR measurements (violet star) and derived from WRF model (red star). Measure gaps are dark-current measurements.

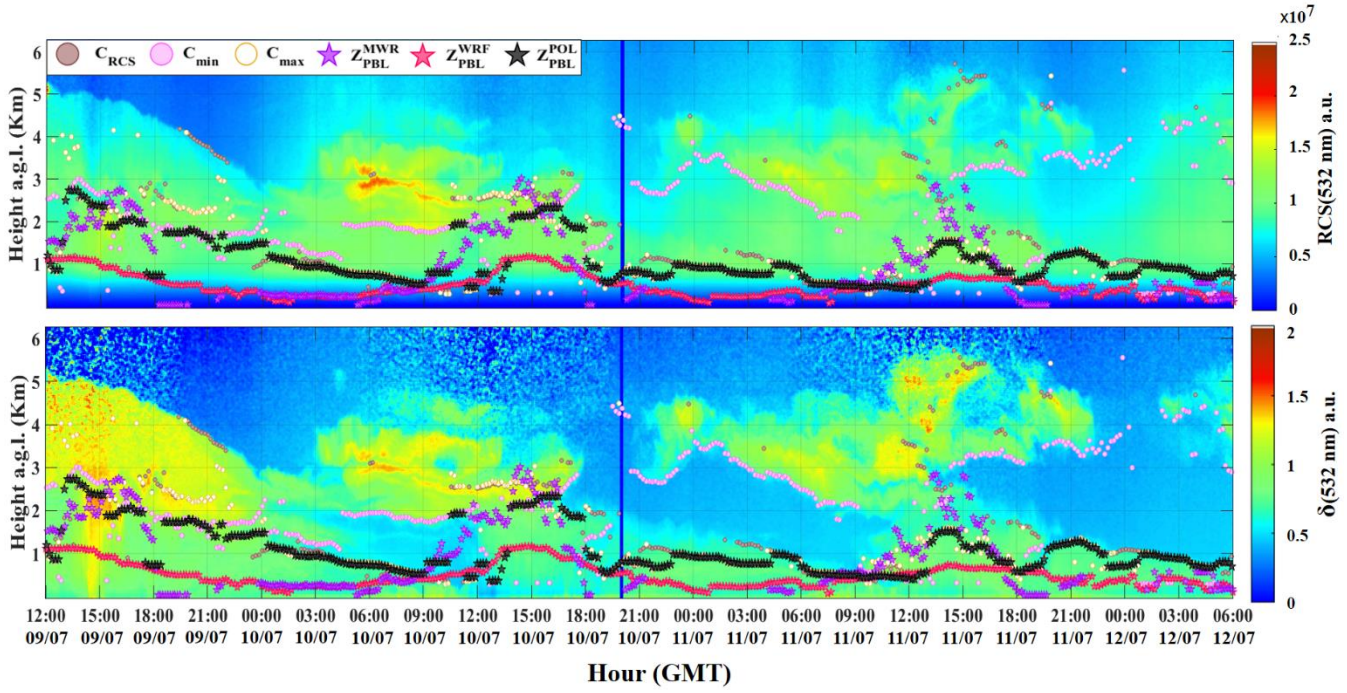

Figure 7: Temporal evolution of the range corrected signal (RCS) (top) and the perpendicular-to-parallel signal ratio (δ) (bottom) in the period 12:00 9 July – 06:00 12 July 2012 (colour maps). The scatter plots represent the candidate for z_{PBL}: C_{RCS} (brown dot), C_{min} (pink dot) and C_{max} (ochre dot). The z_{PBL} determined with POLARIS (black star), by the parcel method using MWR measurements (violet star) and derived from WRF model (red star). Measure gap is dark-current measurement.